Thermodynamic properties of quantum sine-Gordon spin chain system $KCuGaF_6$

Izumi Umegaki,[1] Hidekazu Tanaka,[1,*] Toshio Ono,[2] Masaki Oshikawa,[3] and Kazumitsu Sakai[4]
[1]*Department of Physics, Tokyo Institute of Technology, Meguro-ku, Tokyo 152-8551, Japan*
[2]*Department of Physics, Osaka Prefecture University, Sakai, Osaka 599-8531, Japan*
[3]*Institute for Solid State Physics, University of Tokyo, Kashiwa, Chiba 277-8581, Japan*
[4]*Institute of Physics, University of Tokyo, Meguro-ku, Tokyo 153-8902, Japan*
(Received 18 December 2011; revised manuscript received 21 March 2012; published 24 April 2012)

We investigated the thermodynamic properties of the spin-1/2 one-dimensional Heisenberg antiferromagnet $KCuGaF_6$ by measuring the specific heat in magnetic fields. When this compound is subjected to a uniform magnetic field $\boldsymbol{H}$, a transverse staggered magnetic field $\boldsymbol{h}$ is induced in this compound owing to the staggered component of the $\boldsymbol{g}$ tensor and the Dzyaloshinskii-Moriya interaction with an alternating $\boldsymbol{D}$ vector. Consequently, the quantum sine-Gordon (SG) model is an effective model of this compound in a uniform magnetic field. In three different field directions, we observed a magnetic-field-induced gap, which increases with H. We analyzed experimental results using specific heat theory based on quantum SG theory. The thermodynamic property for $H \parallel c$ is very well described in terms of the elementary excitations characteristic of the quantum SG model, while for the other field directions significant contributions from other excitation modes beyond the framework of the quantum SG model were observed. For $H \parallel b$, a quantum phase transition between gapless and gapped ground states was observed.

DOI: 10.1103/PhysRevB.85.144423 PACS number(s): 75.10.Jm, 75.10.Pq, 76.30.−v, 76.50.+g

I. INTRODUCTION

One-dimensional (1D) quantum systems have attracted considerable attention for a long time because of various phenomena resulting from the strong quantum fluctuations characteristic of the 1D systems. In particular, the $S = 1/2$ antiferromagnetic Heisenberg chain (AFHC) has been closely studied theoretically. Using the Bethe ansatz, the dispersion relation of the lowest excitation for the $S = 1/2$ uniform AFHC, which is known as the des Cloizeaux and Pearson (dCP) mode, has been calculated exactly.[1,2] The two-spinon contribution to magnetic excitations has also been calculated.[3,4] The energy of the dCP mode is different from the result obtained by linear spin wave theory[5,6] by a factor of $\pi/2$, which was verified by inelastic neutron scattering measurements.[7,8] Accurate calculations[9,10] and inelastic neutron scattering measurements[11] showed that low-energy excitations in a magnetic field cannot be described even qualitatively by linear spin wave theory. The calculated dispersion relation demonstrated that gapless excitations occur at incommensurate wave vectors $q = \pm 2\pi m(H) \equiv \pm q_0$ and $\pi \pm q_0$ in addition to at $q = 0$ and π, where $m(H)$ is the magnetization per site in the unit of $g\mu_B$.

By means of neutron inelastic scattering and specific heat measurements, Dender *et al.*[12] observed an unexpected magnetic-field-induced incommensurate gap in $Cu(C_6H_5COO)_2{\cdot}3H_2O$, abbreviated to copper benzoate, which is known as an $S = 1/2$ 1D antiferromagnet with good one-dimensionality.[13–15] This problem was discussed by Oshikawa and Affleck[16–18] on the basis of the effective Hamiltonian expressed as

$$\mathcal{H} = \sum_i \left[J\boldsymbol{S}_i \cdot \boldsymbol{S}_{i+1} - g\mu_B H S_i^z - (-1)^i g\mu_B h S_i^x \right], \quad (1)$$

where h is the transverse staggered field induced by the external field H. The staggered field on the ith site $\boldsymbol{h}_i$ originates from the staggered component of the $\boldsymbol{g}$ tensor $(-1)^i \boldsymbol{g}_s$ and the Dzyaloshinskii-Moriya (DM) interaction[19] with the alternating $\boldsymbol{D}_i$ vector $(-1)^i \boldsymbol{D}$ and is expressed as

$$\boldsymbol{h}_i \simeq (-1)^i \left[\frac{\boldsymbol{g}_s}{g_u} \boldsymbol{H} + \frac{\boldsymbol{H}}{2J} \times \boldsymbol{D} \right], \quad (2)$$

where g_u is the uniform g factor.[17] Because the $\boldsymbol{g}_s$ tensor and $\boldsymbol{D}$ vector are anisotropic, the proportionality coefficient $c_s = h/H$ depends on the field direction.

Using the field-theoretical approach, Oshikawa and Affleck[16,17] demonstrated that the model given by Eq. (1) can be mapped onto the quantum sine-Gordon (SG) model with Lagrangian density

$$\mathcal{L} = \frac{1}{2} \left[\left(\frac{\partial \phi}{\partial t} \right)^2 - (vJ)^2 \left(\frac{\partial \phi}{\partial x} \right)^2 \right] + hC \cos(2\pi R\tilde{\phi}), \quad (3)$$

where ϕ is the canonical Bose field, $\tilde{\phi}$ is the dual field, R is the compactification radius, v is the dimensionless spin wave velocity, and C is a coupling constant. The dual field $\tilde{\phi}$ corresponds to the angle between the transverse component of the spin and the reference direction in a plane perpendicular to the external magnetic field. Owing to the nonlinear term in Eq. (3), all the excitations are gapped as illustrated in Fig. 1.

The elementary excitations characteristic of the quantum SG model are the soliton, antisoliton, and breather excitations. The soliton excitation corresponds to the excitation at $q = \pm q_0$ and $\pi \pm q_0$ and is classically described as the local rotation of the spin in a plane perpendicular to the magnetic field, and the antisoliton excitation corresponds to the inverse rotation of the spin. The breather corresponds to the bound state of the soliton and the antisoliton as reducing their energies with $\tilde{\phi} \simeq 0$. Oshikawa and Affleck[16–18] showed that the magnetic-field-induced gap corresponding to the soliton energy is proportional to $H^{2/3}$. The field dependence of the gap is in good agreement with the experimental result observed for copper benzoate.[12] On the basis of quantum SG theory,[18] they also provided a good

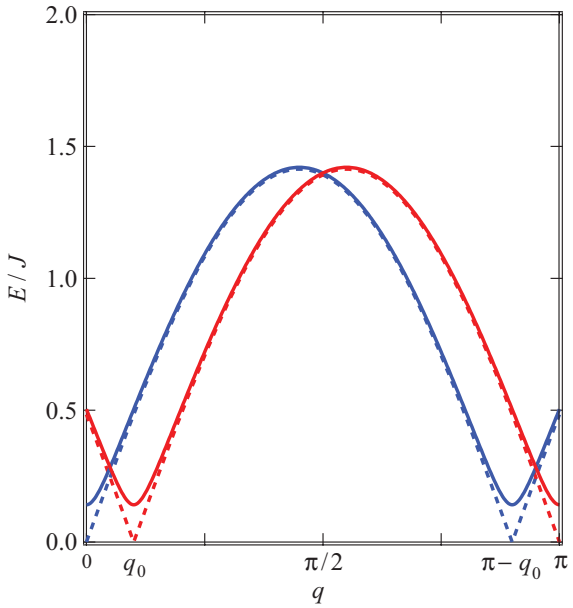

FIG. 1. (Color online) Schematic view of the lowest-energy excitations of model (1) in a nonzero magnetic field for $\boldsymbol{h}=0$ (dashed lines) and $\boldsymbol{h}\neq 0$ (solid lines). There are two excitation branches (colored red and blue). Gapless excitations at $q=0$ and at incommensurate waves $q=\pm q_0$ for $\boldsymbol{h}=0$ have finite gaps for $\boldsymbol{h}\neq 0$. The maximum excitation energy at $q=(\pi\pm q_0)/2$ decreases from $\pi/2$ with increasing magnetic field and becomes zero at $H=2J/(g\mu_B)$.[10]

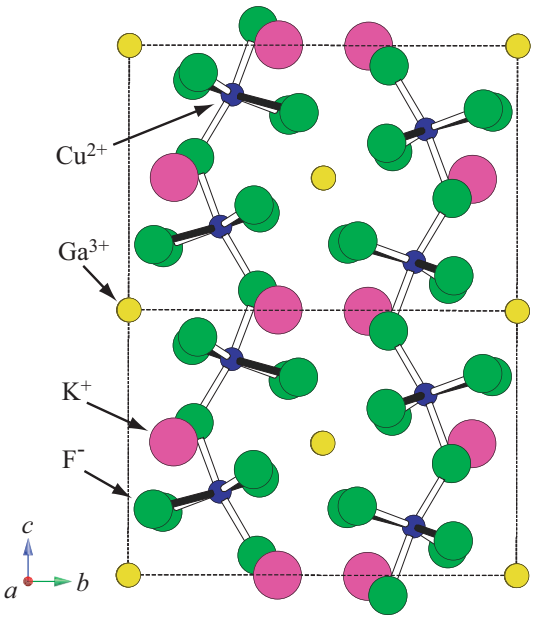

FIG. 2. (Color online) Crystal structure of $KCuGaF_6$ viewed along the a axis. Dotted lines denote the chemical unit cell. Solid and open bonds, respectively, denote the elongated and compressed axes of CuF_6 octahedra.

description for the resonance field of electron spin resonance (ESR) obtained by Oshima *et al.*[20]

The elementary excitations in copper benzoate were investigated in detail using high-frequency ESR.[21,22] In addition to copper benzoate, the following substances are known to be described by the effective model given by Eq. (1): Yb_4As_3,[23–25] $PM{\cdot}Cu(NO_3)_2{\cdot}(H_2O)_2$ (PM, pyrimidine)[26–30] and $CuCl_2{\cdot}2[(CD_3)_2SO]$.[31–33] Because the elementary excitations and thermodynamic properties of quantum SG systems have been of great interest, numerous theoretical investigations have been published,[34–45] and the theoretical results have been used to analyze experimental results on the above-mentioned substances. Moreover, new experiments have been proposed on the basis of theoretical results.[28,46–48]

$KCuGaF_6$ is an $S=1/2$ AFHC system, which is represented by the effective model given by Eq. (1) in a magnetic field.[49,50] $KCuGaF_6$ is composed of corner-sharing CuF_6 octahedra running along the c axis, as shown in Fig. 2.[51] The CuF_6 octahedra are elongated perpendicular to the chain direction, which is parallel to the c axis, owing to the Jahn-Teller effect. Consequently, the hole orbitals of Cu^{2+} ions are linked along the chain direction through the p orbitals of F^- ions, which leads to a strong antiferromagnetic exchange interaction along the c direction of $J/k_B=103\,\mathrm{K}\pm 2\,\mathrm{K}$.[49,50] The elongated and compressed principal axes of the octahedra alternate along the chain direction, as shown by the solid and open bonds in Fig. 2, respectively. This gives rise to the staggered component of the $\boldsymbol{g}$ tensor and the DM interaction with the alternating $\boldsymbol{D}$ vector. Because of the c glide plane at $\pm b/4$, the ac plane component of the $\boldsymbol{D}_i$ vector alternates along the chain direction but the b component does not. Thus, the $\boldsymbol{D}_i$ vector should be expressed as

$$\boldsymbol{D}_i=\left[(-1)^i D_x, D_y, (-1)^i D_z\right], \tag{4}$$

where the x, y, and z axes are chosen to be parallel to the $a^*(\perp b,c)$, b, and c axes, respectively. For these reasons, the staggered transverse magnetic field $\boldsymbol{h}_i$ is induced, when this compound is subjected to an external magnetic field $\boldsymbol{H}$. If the y component D_y is negligible, then the $\boldsymbol{D}_i$ vector is expressed as $\boldsymbol{D}_i=(-1)^i\boldsymbol{D}$. The classical spin arrangements for the staggered and uniform $\boldsymbol{D}$ vectors are the canted Néel state and the spiral state, respectively.

$KCuGaF_6$ differs from other quantum SG substances in its large exchange interaction of $J/k_B=103$ K and its wide range of the proportionality coefficient, $c_s=0.03$–0.18.[49,50] Thus, $KCuGaF_6$ is expected to be suitable for obtaining a comprehensive understanding of the systems described by model (1). In a previous paper,[50] we observed as many as about ten ESR modes in $KCuGaF_6$ and found that most of the ESR modes can be very well explained by quantum SG field theory.[17,40] The magnetic-field-induced gap in $KCuGaF_6$ was also confirmed by NMR measurement and a gap proportional to $H^{2/3}$ was observed for $H\parallel c$.[52]

Specific heat measurement is a powerful tool necessary for obtaining a comprehensive understanding of the excitation nature. In the present paper, we report the results of specific heat measurements on $KCuGaF_6$ in three different field directions. Experimental results are analyzed by performing calculations based on quantum SG field theory. As shown below, the specific heat of $KCuGaF_6$ in a magnetic field can be basically understood in terms of quantum SG field theory. However, we found that additional excitation modes, whose origins are not known, make significant contributions to the specific heat. This paper is organized as follows: in

Sec. II, we summarize the theory of elementary excitations and specific heat in the quantum SG model. Experimental details are reported in Sec. III. The experimental results, their analyses, and a discussion are given in Sec. IV. Section V is devoted to a conclusion.

II. ELEMENTARY EXCITATIONS AND SPECIFIC HEAT IN QUANTUM SG MODEL

The elementary excitations characteristic of quantum SG model are solitons and antisolitons and their bound states called breathers.[16,17] In field-theoretical language, the excitation energies are expressed as the masses of these quasiparticles. Figure 3 illustrates low-energy excitations around $q=0$. Because of the transverse staggered field h induced by the external magnetic field, the gapless excitations at $q=0$, π, $\pm q_0$, and $\pi \pm q_0$ for $h=0$ have finite gaps.

The soliton mass M_s was calculated analytically by Essler *et al.* [40] as

$$\frac{M_s}{J}=\frac{2v}{\sqrt{\pi}}\frac{\Gamma\left(\frac{\xi}{2}\right)}{\Gamma\left(\frac{1+\xi}{2}\right)}\left[\frac{\Gamma\left(\frac{1}{1+\xi}\right)}{\Gamma\left(\frac{\xi}{1+\xi}\right)}\frac{c\pi g\mu_B H}{2vJ}c_s\right]^{(1+\xi)/2}, \quad (5)$$

where $\Gamma(\cdots)$ is the Γ function, v is the dimensionless spin velocity, ξ is a parameter given by $\xi=[2/(\pi R^2)-1]^{-1}$, and c is a parameter depending on the magnetic field. The field dependencies of these parameters are given in the literature;[17,40,53] $v\to\pi/2$, $\xi\to 1/3$, and $c\to 1/2$ for $H\to 0$. This result is applicable in a wide magnetic field range up to the saturation field given by $H_s=2J/(g\mu_B)$.

The breathers M_n $(n=1, 2, \ldots)$ corresponding to the excitations at $q=0$ and π have hierarchical structures labeled by integer n. The mass of the nth breather is given in terms of the soliton mass M_s and parameter ξ as

$$M_n=2M_s\sin\left(\frac{n\pi\xi}{2}\right). \quad (6)$$

The number of breathers is limited by $n\leqslant[\xi^{-1}]$.[17] In a low magnetic field of $g\mu_B H/J<0.5$, breathers up to the third order can exist. The soliton resonance labeled as E_s in Fig. 3 corresponds to the $q=0$ excitation on the excitation branch connected to the soliton and antisoliton. Its energy is given by $E_s\simeq[{M_s}^2+(g\mu_B H)^2]^{1/2}$.[17]

The specific heat in SG field theory can be obtained exactly by taking advantage of its integrability. It has been evaluated by two approaches: the thermodynamic Bethe ansatz (TBA) [54,55] and quantum transfer matrix (QTM) methods.[35,56] In the TBA method, a set of integral equations is derived from the Bethe ansatz. The number of integral equations is finite only at special values of the compactification radius, including the SU(2) symmetric point $R=1/\sqrt{2\pi}$. Thus, the application to the present problem is practically limited to the SU(2) symmetric radius, where the first breather mass M_1 degenerates with soliton mass M_s. Precisely speaking, however, the uniform field H breaks the SU(2) symmetry and thus renormalizes the compactification radius R. This renormalization effect can be taken into account by using the QTM method, which allows the calculation of specific heat for an arbitrary radius. Figure 4 shows the temperature dependence of specific heat of the quantum SG model calculated by the TBA and QTM methods for various soliton mass $M_s=\Delta$.

These calculations of the exact specific heat in SG field theory have been successfully applied in the analysis of the experimental data on PM·Cu$(NO_3)_2\cdot(H_2O)_2$ [26,35] and Yb_4As_3,[24]

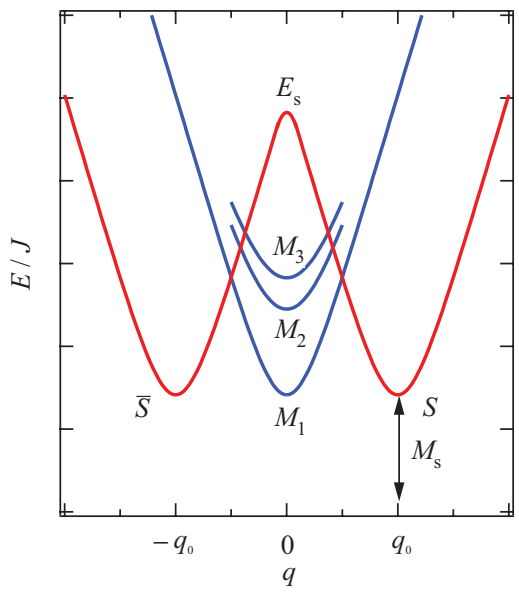

FIG. 3. (Color online) Illustration of low-energy excitations of model (1) around $q=0$. The soliton, antisoliton, soliton resonance, and three breathers are labeled as S, $\bar{S}$, E_s, and M_i ($i=1$, 2, and 3), respectively.

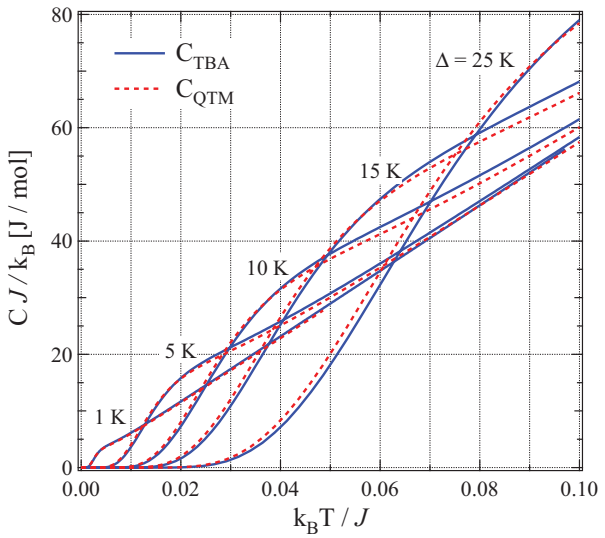

FIG. 4. (Color online) The temperature dependence of the specific heat of the quantum SG model for various soliton mass $M_s=\Delta$. Solid and dashed lines denote the specific heat calculated by the TBA and QTM methods, respectively, with $v=\pi/2$. Note that the dimensionless spin wave velocity v is insensitive to the external magnetic field for $g\mu_B H/J\ll 1$.

which exhibit a field-induced gap similar to that in the present system.

III. EXPERIMENTAL DETAILS

$KCuGaF_6$ single crystals were grown by the horizontal Bridgman method from the melt of an equimolar mixture of KF, CuF_2, and GaF_3 packed into a Pt (platinum) tube of 10 or 15 mm in inner diameter and 100 mm in length. The materials were dehydrated by heating in vacuum at about 100 °C for 3 days. One end of the Pt tube was welded and the other end was tightly folded with pliers. The temperature at the center of a furnace was set at 750 °C and was decreased at a rate of 1 °C/h to 500 °C. Transparent light-pink crystals with a maximum size of $10 \times 15 \times 5$ mm^3 were obtained. These crystals were identified as $KCuGaF_6$ by x-ray powder diffraction analysis.

The crystallographic a, b, and c axes were determined by x-ray single-crystal diffraction. $KCuGaF_6$ crystals are cleaved along the (1, 1, 0) plane. The magnetic susceptibilities χ_a, χ_b, and χ_c are anisotropic below 50 K because of the DM interaction.[50] The magnitudes of the susceptibilities below 50 K decrease in the order $\chi_c > \chi_b > \chi_a$. Thus, the crystallographic axes can be identified from the susceptibility measurements. Specific heat measurements were carried out down to 0.35 K in a magnetic field of up to 9 T using a Physical Property Measurement System (Quantum Design, PPMS). Magnetic fields were applied along the a, b, and c axes. The error is 5% in the absolute value and less than 1% in the relative value in the temperature variation. The error in the absolute value mainly arises from the error in measurement of the sample mass. Then, we obtained C_{total} at zero magnetic field by averaging results on several different samples. The sets of data at finite magnetic fields for three different field directions were calibrated using the C_{total} at zero magnetic field.

IV. RESULTS AND DISCUSSION

Figure 5 shows the low-temperature total specific heat C_{total} measured at zero magnetic field. No magnetic ordering was observed down to 0.35 K, which verifies the good one-dimensionality of the present system. C_{total} is almost proportional to temperature below 4 K, which is a characteristic of the $S = 1/2$ AFHC.[57,58] To evaluate the lattice contribution, we used the theoretical specific heat of the $S = 1/2$ AFHC.[57,58] For $k_B T/J < 0.1$, the specific heat of the $S = 1/2$ AFHC is approximately expressed as

$$C_{\text{AFHC}} = \frac{2R_0 k_B T}{3J}, \tag{7}$$

where R_0 is the gas constant and the spin state is equivalent to the Tomonaga-Luttinger liquid (TLL). C_{total} is the total of the magnetic C_{mag} and lattice C_{lattice} contributions. The solid line in Fig. 5 indicates the theoretical specific heat C_{AFHC} calculated with $J/k_B = 103$ K. The lattice contribution C_{lattice} shown by the dashed line in Fig. 5 was obtained by subtracting C_{AFHC} from C_{total}. The magnetic specific heat in a finite magnetic field was obtained by subtracting the lattice C_{lattice} from the total specific heat C_{total}.

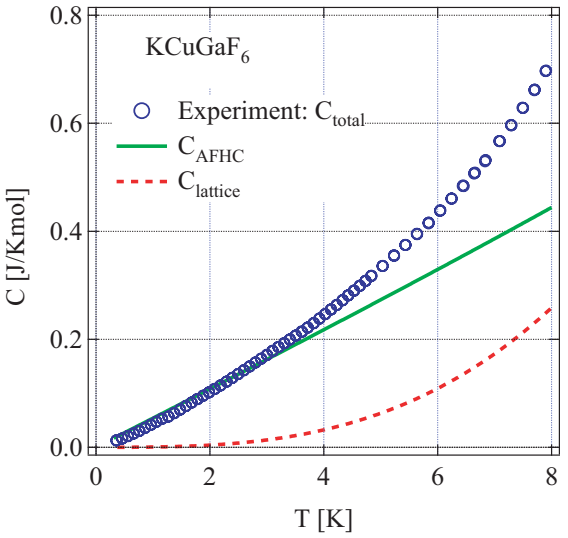

FIG. 5. (Color online) Low-temperature total specific heat C_{total} measured at zero magnetic field. Specific heat data are plotted as open circles. C_{AFHC} is the theoretical low-temperature specific heat given by Eq. (7) with $J/k_B = 103$ K, and C_{lattice} is the lattice contribution estimated by subtracting C_{AFHC} from C_{total}.

Figure 6 shows the low-temperature magnetic specific heat C_{mag} obtained at various magnetic fields parallel to the c axis. For this field direction, the proportionality coefficient $c_s = h/H$ is the largest among the three directions and $c_s = 0.178 \pm 0.002$. In a finite magnetic field, C_{mag} increases exponentially with increasing temperature, which indicates the emergence of a magnetic-field-induced gap. With further increasing temperature, C_{mag} exhibits a rounded shoulder and increases linearly. The shoulder shifts to a higher temperature and becomes broader as the magnetic field increases. This shows that the gap increases with the magnetic field.

We analyzed the experimental results using the exact specific heat in SG field theory. To verify the accuracy of the calculation and to determine the effect of the field renormalization of the compactification radius R, we compared the experimental data with the theoretical specific heats obtained by the TBA and QTM methods. In the TBA calculation, R is fixed to the SU(2) symmetric radius as discussed above. In the QTM calculation, R is obtained as a function of H using the exact Bethe ansatz solution of the Heisenberg chain without the staggered field.[36] Thus, the only adjustable fitting parameter is the soliton mass $M_s = \Delta$ in both calculations.

The solid lines in Fig. 6 show the fits by $C_{\text{TBA}}(\Delta)$ with the soliton mass shown in Fig. 7. On the whole, the experimental specific heat for $H \parallel c$ is well described by the theory based on quantum SG field theory, although some discrepancy is observed. The following three factors may have led to the discrepancy between the experimental and the theoretical results: the breaking of the SU(2) symmetry, the error in the estimation of the lattice contribution C_{lattice}, and the effect of unknown excitation modes observed in previous ESR measurements.[50]

The effect of breaking the SU(2) symmetry is determined by comparing the TBA calculation with R fixed at $1/\sqrt{2\pi}$ and the QTM calculation with the renormalized R. Figure 8

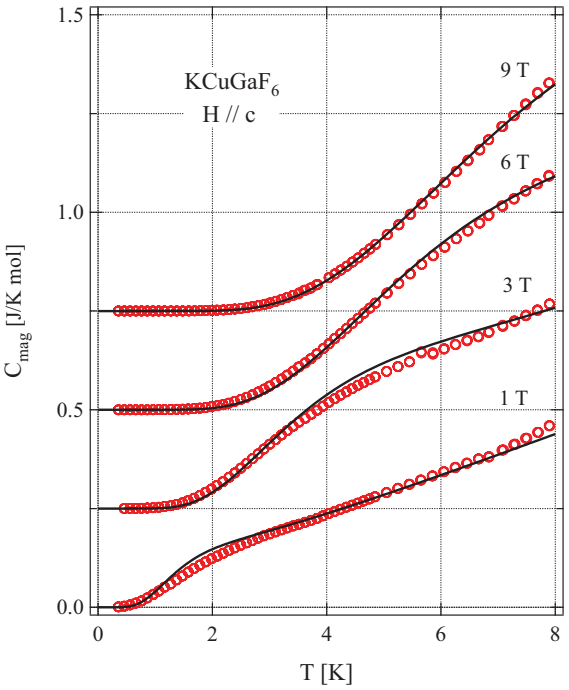

FIG. 6. (Color online) Temperature dependence of magnetic specific heat $C_{\rm mag}$ measured at $H = 1$, 3, 6, and 9 T for $H \parallel c$. Each set of data is shifted upward by a multiple of 0.25 J/(K mol). Open circles indicate experimental data and solid lines are the theoretical specific heat $C_{\rm TBA}(\Delta)$ based on quantum SG field theory fitted with the soliton mass Δ shown in Fig. 7.

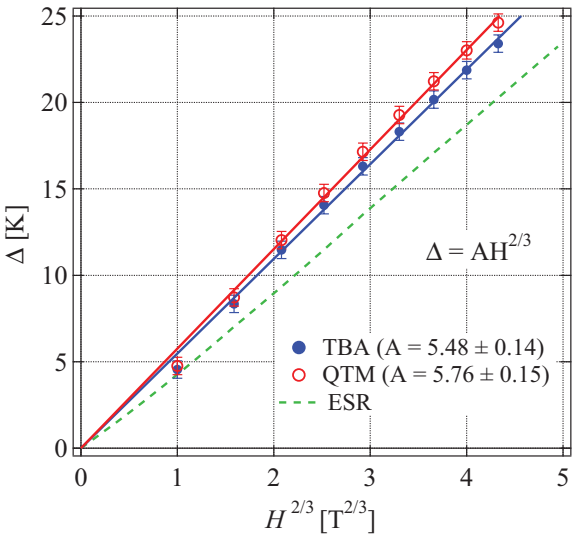

FIG. 7. (Color online) Soliton mass $\Delta\,(\equiv M_{\rm s})$ for $H \parallel c$ as a function of $H^{2/3}$ obtained from the fits of the theoretical specific heat calculated using the TBA (solid circles) and QTM (open circles) methods. The dashed line shows M_s in Eq. (5) with $J/k_{\rm B} = 103$ K and the proportionality coefficient obtained by ESR measurements as $c_s = 0.178$.

shows a comparison between the results of analyses based on the TBA and QTM methods. As shown in Figs. 7 and 8, the temperature dependencies of the specific heat and the soliton masses obtained from both methods are similar. This means that, in the present magnetic field range, the effect of the renormalization of R is not important and the system can be well approximated by the SU(2) symmetric radius $R = 1/\sqrt{2\pi}$. In fact, in the present material, the exchange interaction $J/k_{\rm B} = 103$ K is dominant over the magnetic field used in the experiments.[49,50] In addition, the specific heat is not very sensitive to a small change in R.

The soliton masses Δ for $H \parallel c$ evaluated from the analyses using the TBA and QTM methods are shown in Fig. 7 as a function of $H^{2/3}$. It is clear that Δ is proportional to $H^{2/3}$. This relation can be derived by setting $\xi = 1/3$ in Eq. (5). Note that in the linear spin wave theory, the energy gap exhibits the field dependence of $\Delta \propto H^{1/2}$. Therefore, the field dependence of the soliton mass for $H \parallel c$ agrees well with that in quantum SG field theory.

The dashed line in Fig. 7 indicates the soliton mass Δ obtained from previous ESR measurements.[50] The soliton mass obtained from the specific heat measurements is 1.2 times as large as that obtained from the ESR measurements. The overestimation of the soliton mass is attributed to the unknown higher-energy excitation modes U_2 and U_3 observed in ESR measurements.[50] In another quantum SG system PM·Cu$(NO_3)_2\cdot(H_2O)_2$, the ratio of the gap obtained from specific heat measurements[26] to that obtained from ESR measurements[27] is similar to that observed for $KCuGaF_6$.

While the small disagreement in the soliton mass is found, the experimental $C_{\rm mag}$ for $H \parallel c$ is well described within the framework of quantum SG field theory, as shown in Figs. 6 and 8.

Next, we show in Fig. 9 the low-temperature magnetic specific heat $C_{\rm mag}$ obtained at various magnetic fields for $H \parallel a$. For this field direction, the proportionality coefficient is the smallest and $c_{\rm s} = 0.031 \pm 0.001$.[50] From the exponential increase in $C_{\rm mag}$, we see that the gap opens in a magnetic field. However, because of the small proportionality coefficient $c_{\rm s}$,

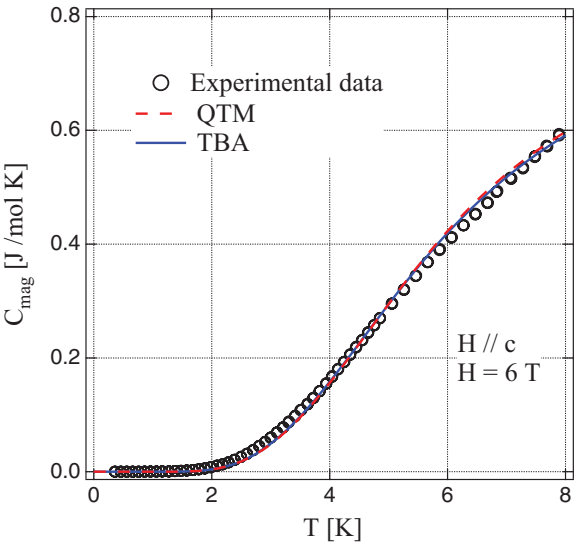

FIG. 8. (Color online) Analyses of the specific heat obtained using the TBA and QTM methods based on quantum SG field theory. Circles show the magnetic specific heat measured at $H = 6$ T for $H \parallel c$. Dashed and solid lines indicate the theoretical specific heat calculated using the TBA and QTM methods, respectively.

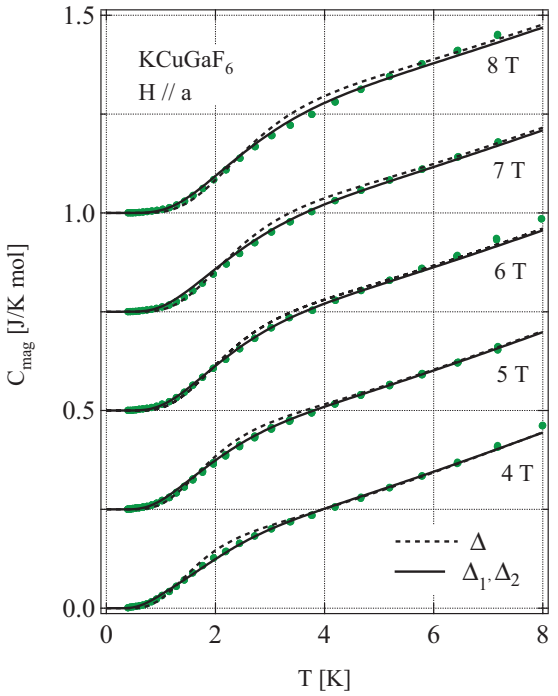

FIG. 9. (Color online) Magnetic specific heat $C_{\rm mag}$ measured for $H \parallel a$. Each set of data is shifted upward by a multiple of 0.25 J/(K mol). Dashed lines denote fits by $C_{\rm TBA}(\Delta)$ with a single soliton mass Δ, while solid lines indicate fits using Eq. (8) with the two gaps Δ_1 and Δ_2 shown in Fig. 10.

the magnitude of the gap is much smaller than that for $H \parallel c$ at the same magnetic field. First, we fitted the theoretical specific heat $C_{\rm TBA}(\Delta)$ to the experimental data. The soliton mass Δ obtained is plotted in Fig. 10 as a function of $H^{2/3}$. As shown by the dashed lines in Fig. 9, some discrepancy was observed between the experimental and theoretical results. A similar discrepancy was also observed in copper benzoate when an external field was applied along the a'' direction, for which the gap becomes smallest.[35] Although Δ is proportional to $H^{2/3}$, as predicted by quantum field theory, its magnitude is 1.5 times as large as that obtained from the ESR measurements. It is considered that this discrepancy for $KCuGaF_6$ arises from the higher-energy unknown mode U_1 and multiple excitation modes C_n, which cannot be explained within the framework of quantum SG field theory.[50]

The energy of the U_1 mode observed for $H \parallel a$ is larger than the mass of the first breather and is comparable to that of the second and third breathers. The C_n modes are multiple excitations of the $E_{\rm s}$ and the breathers, whose energies are given by $E_{\rm s} + M_n$. Note that these modes were also observed in ESR measurements on $PM{\cdot}Cu(NO_3)_2{\cdot}(H_2O)_2$.[27] These excitations can contribute to the magnetic specific heat because they are excitations from the ground state. Then, assuming that the contribution of these higher-energy excitations is effectively represented as $C_{\rm TBA}(\Delta_2)$ with the secondary gap Δ_2, we express the theoretical specific heat as

$$C_{\rm mag}^{\rm eff} = \tfrac{1}{2}[C_{\rm TBA}(\Delta_1) + C_{\rm TBA}(\Delta_2)]. \qquad (8)$$

The first term expresses the contribution of the excitations of the quantum SG model, while the second term expresses the

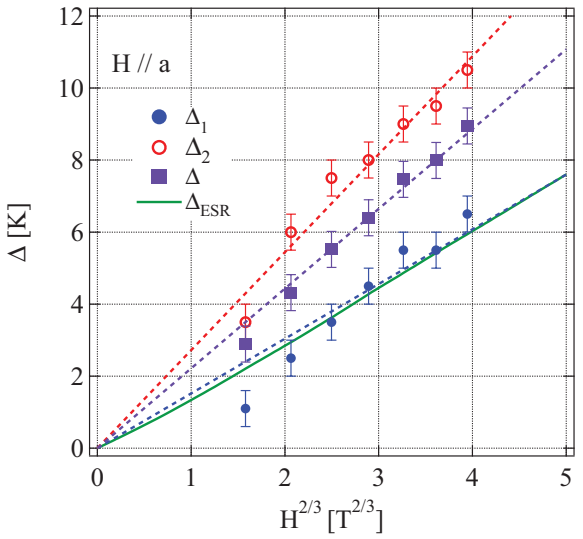

FIG. 10. (Color online) Soliton mass $\Delta\,(\equiv M_{\rm s})$ for $H \parallel a$ as a function of $H^{2/3}$ obtained from fits of the theoretical specific heat $C_{\rm TBA}(\Delta)$ (squares). Closed and open circles indicate the gaps Δ_1 and Δ_2 obtained by fits using Eq. (8), respectively. Solid line indicates M_s in Eq. (5) with $J/k_{\rm B} = 103$ K and the proportionality coefficient obtained by ESR measurements as $c_s = 0.031$.

contribution of other higher-energy excitations. The primary gap Δ_1 corresponds to the true soliton mass. The solid lines in Fig. 9 show fits using Eq. (8). The experimental specific heat in various magnetic fields for $H \parallel a$ ia well described by $C_{\rm mag}^{\rm eff}$. The two gaps, Δ_1 and Δ_2, obtained from the fits are plotted as functions of $H^{2/3}$ in Fig. 10 together with the soliton mass

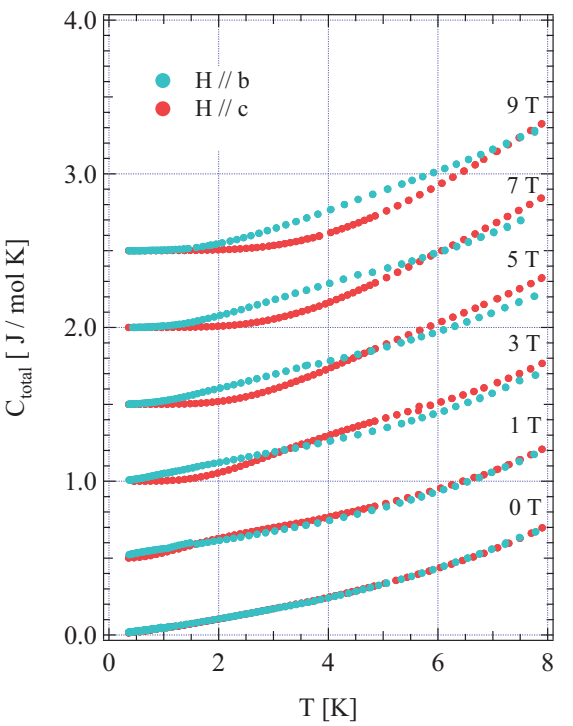

FIG. 11. (Color online) Comparison between total specific heat $C_{\rm total}$ for $H \parallel b$ and $H \parallel c$ measured at various magnetic fields. Each set of data is shifted upward by a multiple of 0.5 J/(mol K).

estimated from the ESR measurements.[50] Both energy gaps are proportional to $H^{2/3}$ for $H \geqslant 3$ T. The primary gap Δ_1 coincides with the soliton mass estimated from the previous ESR measurements. This means that the lower excitations for $H \parallel a$ can be understood within the framework of quantum SG field theory.

Figure 11 shows the temperature dependencies of the total specific heat $C_{\rm total}$ for $H \parallel b$ and $H \parallel c$, for which the proportionality coefficients are $c_s = 0.160 \pm 0.002$ and 0.178 ± 0.002, respectively.[50] The values of magnetic specific heat for these two field directions were expected to be similar, because the proportionality coefficients are close to each other. However, the values of specific heats are clearly different, as shown in Fig. 11. It is apparent that the magnetic-field-induced gap for $H \parallel b$ is much smaller than that for $H \parallel c$. A notable feature is that the specific heat for $H \parallel b$ is almost linear in temperature for $H \leqslant 2$ T. This indicates that the ground state is gapless at low magnetic fields. The low-magnetic-field specific heat does not exhibit an anomaly indicative of 3D ordering down to 0.35 K, although the ground state appears gapless. These observations appear to be consistent with the result of previous ESR measurements for $H \parallel b$, where we observed an intense unknown U_4 mode with resonance frequency proportional to $H - H_c$ with $H_c \simeq 2.5$ T.[50]

Figure 12 shows the magnetic specific heat measured at various magnetic fields for $H \parallel b$. Fitting of the theoretical specific heat $C_{\rm TBA}(\Delta)$ to the experimental data was not successful, as shown by the dashed lines in Fig. 12, and contrary to the case of $H \parallel a$, we obtained a soliton mass Δ considerably smaller than that estimated from ESR measurements (see Fig. 13). The soliton mass Δ is not proportional to $H^{2/3}$ but can be expressed as $\Delta = A\{H^{2/3} - H_c(0)^{2/3}\}$ with $A = 4.33 \pm 0.33$ and $H_c(0) = 1.51 \pm 0.05$ T. In previous ESR measurements, we observed three unknown modes, U_1, U_2, and U_3, whose excitation energies are close to or lower than the first breather mass added to in the U_4 mode.[50] The unexpectedly small soliton mass obtained from the present specific heat measurements should be due to these low-energy

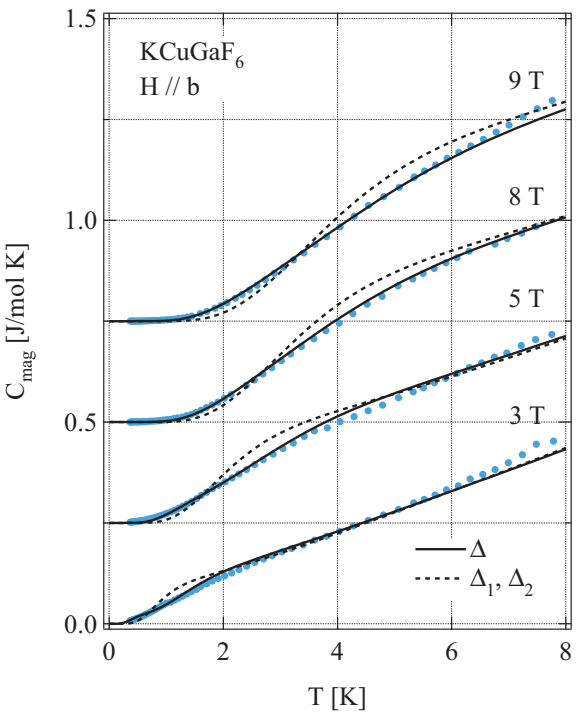

FIG. 12. (Color online) Magnetic specific heat $C_{\rm mag}$ measured for $H \parallel b$. Each set of data is shifted upward by a multiple of 0.25 J/(mol K). Dashed lines show fits by the theoretical specific heat $C_{\rm TBA}(\Delta)$, while solid lines indicate fits using Eq. (8).

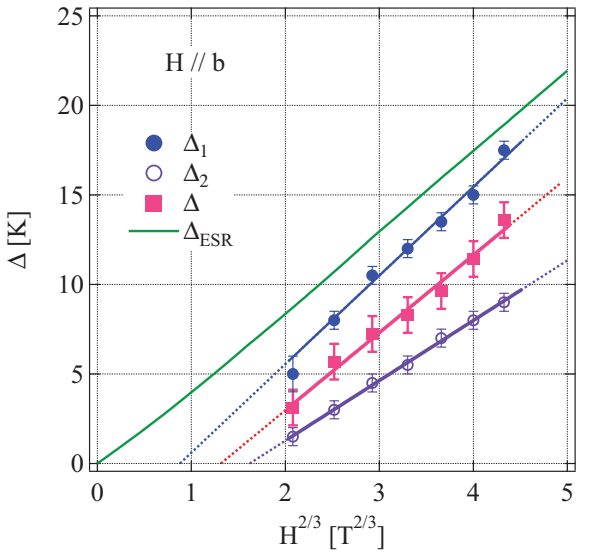

FIG. 13. (Color online) Soliton mass $\Delta\,(\equiv M_s)$ for $H \parallel b$ as a function of $H^{2/3}$ obtained from the fits of the theoretical specific heat $C_{\rm TBA}(\Delta)$ (solid squares). Solid and open circles indicate the gaps Δ_1 and Δ_2 obtained by fits using Eq. (8), respectively. The solid line indicates M_s in Eq. (5) with $J/k_B = 103$ K and the proportionality coefficient obtained by ESR measurements as $c_s = 0.16$.

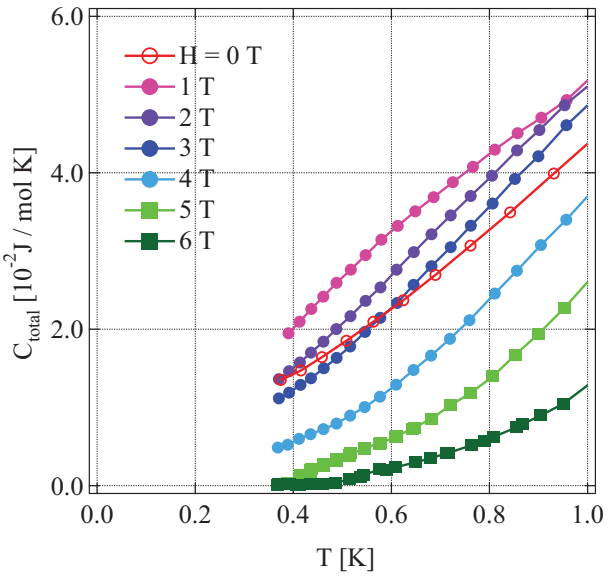

FIG. 14. (Color online) Low-temperature total specific heat $C_{\rm total}$ measured at various magnetic fields for $H \parallel b$. Open circles indicate $C_{\rm total}$ at zero field. Solid symbols indicate $C_{\rm total}$ in nonzero magnetic fields.

unknown modes. Then, assuming that the contribution of these unknown modes is effectively expressed in terms of the secondary gap Δ_2, which is much smaller than the soliton mass Δ_1, we describe the magnetic specific heat by Eq. (8), as in the case of $H \parallel a$. The solid lines in Fig. 12 indicate the fits using Eq. (8) with the two gaps shown in Fig. 13. The experimental value of $C_{\rm mag}$ for $H \parallel b$ is effectively described by Eq. (8). Similar to the soliton gap Δ obtained from the fit by $C_{\rm TBA}(\Delta)$, both the primary gap Δ_1 and the secondary gap Δ_2 obtained for $H \geqslant 3$ T are expressed as $\Delta_i = A\{H^{2/3} - H_{\rm c}(i)^{2/3}\}$ ($i = 1$ and 2) with $H_{\rm c}(1) = 0.82 \pm 0.13$ T and $H_{\rm c}(2) = 2.06 \pm 0.01$ T. This value of $H_{\rm c}(2)$ is close to the critical field $H_{\rm c} \simeq 2.5$ T observed in ESR measurements for $H \parallel b$.[50] The values of A are 4.95 ± 0.40 and 3.36 ± 0.09, respectively.

In Fig. 14, we show the total specific heat $C_{\rm total}$ measured below 1 K at various magnetic fields. In this temperature range, the lattice contribution $C_{\rm lattice}$ is negligible. $C_{\rm total}$ appears to be linear in temperature for $H \leqslant 3$ T, while for $H \geqslant 5$ T, $C_{\rm total}$ exhibits exponential temperature dependence. This indicates that the gapless ground state changes into a gapped state between 3 and 5 T. To confirm the magnetic-field-induced quantum phase transition, we performed a field scan of specific heat at $T = 0.4$ K. The result is shown in Fig. 15 with the sum of $C_{\rm mag}$ and $C_{\rm lattice}$ calculated using the TBA results shown in Fig. 4 with the gap $\Delta_{\rm ESR}$ obtained from the ESR measurements. The total specific heat $C_{\rm total}$ has a peak at $H = 0.6$ T and shoulders at $H = 1.8$ and 3 T. No such behavior was observed for $H \parallel a$ and $H \parallel c$. In these field directions, $C_{\rm total}$ at finite magnetic field is always smaller than $C_{\rm total}$ at zero magnetic field at low temperatures, because the magnitude of the field-induced gap increases with increasing magnetic field. With further increasing magnetic field, $C_{\rm total}$ decreases rapidly and becomes almost zero at $H = 5.5$ T. Unlike this result, the calculation shows that $C_{\rm mag}$ monotonously decreases as the magnetic field increases. From these observations, we can deduce that the gapless ground state for $H \parallel b$ becomes a gapped state in between 3 and 5.5 T. The critical field $H_{\rm c}$ is larger than $H_{\rm c} \simeq 2.5$ T observed in ESR measurements.[50] At present, the origins of the low-field gapless state for $H \parallel b$ and the unknown ESR modes that make a large contribution to the specific heat are not clear. The uniform b axis component of the $\boldsymbol{D}$ vector, which gives rise to a helical spin structure or a soliton lattice in a magnetic field,[59] may be responsible for these effects.

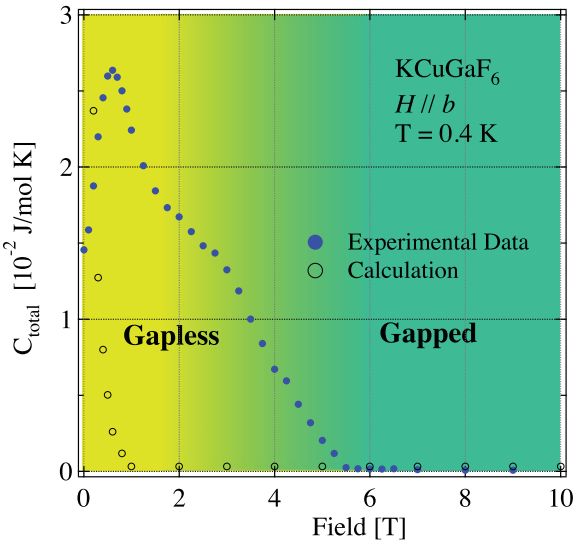

FIG. 15. (Color online) Magnetic field dependence of total specific heat $C_{\rm total}$ measured at $T = 0.4$ K for $H \parallel b$. The quantum phase transition where a gapless ground state changes into a gapped state is observed. Open circles indicate the sum of $C_{\rm lattice}$ and $C_{\rm mag}$ calculated using the TBA calculations shown in Fig. 4 with the gap $\Delta_{\rm ESR}$.

V. CONCLUSION

We have presented results for the specific heat of $KCuGaF_6$ in magnetic fields. It was clearly observed that an excitation gap opens in a magnetic field and increases with increasing magnetic field. Specific heat data were analyzed using two theoretical values of specific heat calculated by the TBA and QTM methods, both of which are based on the quantum SG model. In the TBA method, the SU(2) symmetry is assumed, while in the QTM method, the breaking of the SU(2) symmetry owing to the external magnetic field is taken into account. The specific heat for $H \parallel c$ is well reproduced by these two calculations with the soliton mass close to that obtained from previous ESR measurements. The soliton mass was found to be proportional to $H^{2/3}$. These results indicate that the thermodynamic properties for $H \parallel c$ are well described by quantum SG field theory and that the breaking of the SU(2) symmetry is negligible in our experimental magnetic field range because of the large exchange interaction of $J/k_{\rm B} = 103$ K.

In the cases of $H \parallel a$ and $H \parallel b$, we found a significant contribution of additional excitations that cannot be explained in the framework of quantum SG field theory. For these field directions, we analyzed the specific heat data using Eq. (8), in which the contribution of the unknown excitations is effectively taken into account by assuming a secondary gap Δ_2. For $H \parallel a$, the primary gap Δ_1 agrees with the soliton mass $\Delta_{\rm ESR}$ obtained from the ESR measurements, while for $H \parallel b$, Δ_1 does not agree with $\Delta_{\rm ESR}$. We found that, for $H \parallel b$, the ground state is gapless at low magnetic fields and that with increasing magnetic field a quantum phase transition occurs between gapless and gapped ground states.

ACKNOWLEDGMENTS

The authors would like to acknowledge H. Nojiri, S. C. Furuya, and I. Affleck for useful discussions. This work was supported by a Grant-in-Aid for Scientific Research (A) from the Japan Society for the Promotion of Science and by the Global COE Program "Nanoscience and Quantum Physics" at the Tokyo Institute of Technology, both funded by the Japanese Ministry of Education, Culture, Sports, Science and Technology. I.U. and H.T. were supported by a JSPS Research Fellowship for Young Scientists and a grant from the Mitsubishi Foundation, respectively.

*tanaka@lee.phys.titech.ac.jp.

[1] J. des Cloizeaux and J. J. Pearson, Phys. Rev. **128**, 2131 (1962).
[2] L. D. Faddeev and L. A. Takhtajan, Phys. Lett. A **85**, 375 (1981).
[3] T. Yamada, Prog. Theor. Phys. **41**, 880 (1969).
[4] G. Müller, H. Thomas, H. Beck, and J. C. Bonner, Phys. Rev. B **24**, 1429 (1981).
[5] P. W. Anderson, Phys. Rev. **86**, 694 (1952).
[6] R. Kubo, Phys. Rev. **87**, 568 (1952).
[7] Y. Endoh, G. Shirane, R. J. Birgeneau, P. M. Richards, and S. L. Holt, Phys. Rev. Lett. **32**, 170 (1974).
[8] S. E. Nagler, D. A. Tennant, R. A. Cowley, T. G. Perring, and S. K. Satija, Phys. Rev. B **44**, 12361 (1991).
[9] E. Pytte, Phys. Rev. B **10**, 4637 (1974).
[10] N. Ishimura and H. Shiba, Prog. Theor. Phys. **57**, 1862 (1977).
[11] See Fig. 3 in I. U. Heilmann, G. Shirane, Y. Endoh, R. J. Birgeneau, and S. L. Holt, Phys. Rev. B **18**, 3530 (1978).
[12] D. C. Dender, P. R. Hammar, D. H. Reich, C. Broholm, and G. Aeppli, Phys. Rev. Lett. **79**, 1750 (1997).
[13] M. Date, M. Motokawa, and H. Yamazaki, J. Phys. Soc. Jpn. **18**, 911 (1963).
[14] M. Date, H. Yamazaki, M. Motokawa, and S. Tazawa, Prog. Theor. Phys. Suppl. **46**, 194 (1970).
[15] K. Takeda, Y. Yoshino, K. Matsumoto, and T. Haseda, J. Phys. Soc. Jpn. **49**, 162 (1980).
[16] M. Oshikawa and I. Affleck, Phys. Rev. Lett. **79**, 2883 (1997).
[17] I. Affleck and M. Oshikawa, Phys. Rev. B **60**, 1038 (1999); **62**, 9200(E) (2000).
[18] M. Oshikawa and I. Affleck, Phys. Rev. Lett. **82**, 5136 (1999).
[19] T. Moriya, Phys. Rev. **120**, 91 (1960).
[20] K. Oshima, K. Okuda, and M. Date, J. Phys. Soc. Jpn. **44**, 757 (1978).
[21] T. Asano, H. Nojiri, Y. Inagaki, J. P. Boucher, T. Sakon, Y. Ajiro, and M. Motokawa, Phys. Rev. Lett. **84**, 5880 (2000).
[22] H. Nojiri, Y. Ajiro, T. Asano, and J. P. Boucher, New J. Phys. **8**, 218 (2006).
[23] R. Helfrich, M. Küppen, M. Lang, F. Steglich, and A. Ochiai, J. Magn. Magn. Mater. **177-181**, 309 (1998).
[24] M. Oshikawa, K. Ueda, H. Aoki, A. Ochiai, and M. Kohgi, J. Phys. Soc. Jpn. **68**, 3181 (1999).
[25] M. Kohgi, K. Iwasa, J. M. Mignot, B. Fåk, P. Gegenwart, M. Lang, A. Ochiai, H. Aoki, and T. Suzuki, Phys. Rev. Lett. **86**, 2439 (2001).
[26] R. Feyerherm, S. Abens, D. Günther, T. Ishida, M. Meißner, M. Meschke, T. Nogami, and M. Steiner, J. Phys.: Condens. Matter **12**, 8495 (2000).
[27] S. A. Zvyagin, A. K. Kolezhuk, J. Krzystek, and R. Feyerherm, Phys. Rev. Lett **93**, 027201 (2004).
[28] S. A. Zvyagin, E. Čižmár, M. Ozerov, J. Wosnitza, R. Feyerherm, S. R. Manmana, and F. Mila, Phys. Rev. B **83**, 060409 (2011).
[29] A. U. B. Wolter, H. Rakoto, M. Costes, A. Honecker, W. Brenig, A. Klümper, H.-H. Klauss, F. J. Litterst, R. Feyerherm, D. Jérome, and S. Süllow, Phys. Rev. B **68**, 220406(R) (2003).
[30] A. U. B. Wolter, P. Wzietek, S. Süllow, F. J. Litterst, A. Honecker, W. Brenig, R. Feyerherm, and H.-H. Klauss, Phys. Rev. Lett. **94**, 057204 (2005).
[31] M. Kenzelmann, Y. Chen, C. Broholm, D. H. Reich, and Y. Qiu, Phys. Rev. Lett. **93**, 017204 (2004).
[32] M. Kenzelmann, C. D. Batista, Y. Chen, C. Broholm, D. H. Reich, S. Park, and Y. Qiu, Phys. Rev. B **71**, 094411 (2005).
[33] Y. Chen, M. B. Stone, M. Kenzelmann, C. D. Batista, D. H. Reich, and C. Broholm, Phys. Rev. B **75**, 214409 (2007).
[34] F. H. L. Essler and A. M. Tsvelik, Phys. Rev. B **57**, 10592 (1998).
[35] F. H. L. Essler, Phys. Rev. B **59**, 14376 (1999).
[36] E. Korepin, A. G. Izergin, and N. M. Bogoliubov, *Quantum Inverse Scattering Method, Correlation Functions and Algebraic Bethe Ansatz* (Cambridge University Press, Cambridge, UK, 1993).
[37] J. Lou, S. Qin, C. Chen, Z. Su, and L. Yu, Phys. Rev. B **65**, 064420 (2002).
[38] F. Capraro and C. Gros, Eur. Phys. J. B **29**, 35 (2002).
[39] Y.-J. Wang, F. H. L. Essler, M. Fabrizio, and A. A. Nersesyan, Phys. Rev. B **66**, 024412 (2002).
[40] F. H. L. Essler, A. Furusaki, and T. Hikihara, Phys. Rev. B **68**, 064410 (2003).
[41] J. Z. Zhao, X. Q. Wang, T. Xiang, Z. B. Su, and L. Yu, Phys. Rev. Lett. **90**, 207204 (2003).
[42] J. Lou, C. Chen, J. Zhao, X. Wang, T. Xiang, Z. Su, and L. Yu, Phys. Rev. Lett. **94**, 217207 (2005).
[43] S. Glocke, A. Klümper, H. Rakoto, J. M. Broto, A. U. B. Wolter, and S. Süllow, Phys. Rev. B **73**, 220403(R) (2006).
[44] E. Orignac, R. Citro, S. Capponi, and D. Poilblanc, Phys. Rev. B **76**, 144422 (2007).
[45] I. Kuzmenko and F. H. L. Essler, Phys. Rev. B **79**, 024402 (2009).
[46] H. Karimi and I. Affleck, Phys. Rev. B **84**, 174420 (2011).
[47] B. Xi, S. Hu, J. Zhao, G. Su, B. Normand, and X. Wang, Phys. Rev. B **84**, 134407 (2011).
[48] M. Sato, H. Katsura, and N. Nagaosa, e-print arXiv:1105.2259v1.
[49] R. Morisaki, T. Ono, H. Tanaka, and H. Nojiri, J. Phys. Soc. Jpn. **76**, 063706 (2007).
[50] I. Umegaki, H. Tanaka, T. Ono, H. Uekusa, and H. Nojiri, Phys. Rev. B **79**, 184401 (2009).
[51] P. Dahlke, J. Pebler, and D. Babel, Z. Anorg. Allg. Chem. **631**, 115 (2005).
[52] Y. Mori, T. Goto, I. Umegaki, and H. Tanaka, J. Phys.: Conf. Ser. **302**, 012012 (2010).
[53] T. Hikihara and A. Furusaki, Phys. Rev. B **69**, 064427 (2004).
[54] M. Takahashi and M. Suzuki, Prog. Theor. Phys. **48**, 2187 (1972).
[55] M. Fowler and X. Zotos, Phys. Rev. B **24**, 2634 (1981); **25**, 5806 (1982).
[56] C. Destri and H. J. De Vega, Nucl. Phys. B **438**, 413 (1995).
[57] A. Klümper, Eur. Phys. J. B **5**, 677 (1998).
[58] D. C. Johnston, R. K. Kremer, M. Troyer, X. Wang, A. Klümper, S. L. Bud'ko, A. F. Panchula, and P. C. Canfield, Phys. Rev. B **61**, 9558 (2000).
[59] I. Garate and I. Affleck, Phys. Rev. B **81**, 144419 (2010).